Earth and Planetary Science Letters 545 (2020) 116411

Contents lists available at ScienceDirect

Earth and Planetary Science Letters

www.elsevier.com/locate/epsl

Hydrocarbon migration pathway and methane budget for a Gulf of Mexico natural seep site: Green Canyon 600

C. Johansen [a,*], L. Macelloni [b], M. Natter [c], M. Silva [a], M. Woosley [b], A. Woolsey [d], A.R. Diercks [b], J. Hill [e], R. Viso [e], E. Marty [f,1], V.V. Lobodin [g], W. Shedd [c], S.B. Joye [f], I.R. MacDonald [a]

[a] Florida State University, Tallahassee, FL, USA
[b] School of Ocean, Science and Engineering, University of Southern Mississippi, Stennis Space Center, MS, USA
[c] Bureau of Ocean Energy Management, New Orleans, LA, USA
[d] Mississippi Mineral Resources Institute, University of Mississippi, University, MS, USA
[e] Coastal Carolina University, Conway, SC, USA
[f] University of Georgia, Marine Sciences, Athens, GA, USA
[g] National High Magnetic Field Laboratory, Tallahassee, FL, USA

ARTICLE INFO

Article history:
Received 30 November 2019
Received in revised form 2 June 2020
Accepted 8 June 2020
Available online 27 June 2020
Editor: L. Derry

Keywords:
natural hydrocarbon seeps
migration
methane budget
flux
systems approach

ABSTRACT

Hydrocarbon seeps occur worldwide along continental margins and act as conduits for fluid discharge from the lithosphere to the overlying hydrosphere/atmosphere. The dynamics and rates of hydrocarbon release at cold seeps remain poorly constrained. Seepage enables a variety of processes that alter the seafloor morphology and affect the geochemistry of substrata, supporting diverse and important chemosynthetic communities. Here we merge complementary geochemical (oil fingerprinting), geophysical (deep seismic, subbottom, backscatter, multibeam) and video/imaging (Video Time Lapse Camera, *DSV ALVIN* video, ROV video, AUV photo surveys) data sets to constrain the pathways and magnitudes of methane fluxes from the source reservoir to the seafloor at a well-studied, prolific seep site, Green Canyon (GC) 600 in the Northern Gulf of Mexico. Oil samples from the reservoir, an active vent, and the sea-surface showed compositional similarities consistent with the plumbing system structure identified in seismic data. Spatial distribution of seep indicators such as bacterial mats, microbial communities, methane derived carbonates, and hydrate outcrops, were then used to quantify the total magnitude of methane potentially sequestered in the study domain. Using a systems approach, we combined published values for methane fluxes with data we collected across various scales and resolutions to compile a methane budget for GC600. The system considered for the methane budget is defined as the movement of methane from the salt ridge to the seafloor-water interface for each seep domain, Birthday Candles and Mega Plume. Total estimated input of methane was 2.8×10^8–2.2×10^9 mol/yr in the Birthday Candles domain, and 2.7×10^8–2.3×10^9 in the Mega Plume domain. The combined total output of the system ranged from 3.2×10^5–8.2×10^5 and 3.2×10^6–5.2×10^6 mol/yr respectively for Birthday Candles and Mega Plume domains, leaving a potential surplus (input minus output) of 2.6×10^8–2.3×10^9 mol/yr. Processes that could balance this budget include accumulation of gas hydrate and sediment free-gas, and the underestimated potential of biological sinks such as methane oxidation.

1. Introduction

Natural seeps occur across diverse settings worldwide. Indicators of fluid flow at the seafloor include physical structures such as mud volcanoes, gas hydrate mounds, authigenic carbonate outcrops, seafloor depressions (e.g. pockmarks), bubble plumes containing oily and gas containing droplets (Judd and Hovland, 2009), and complex chemosynthetic communities (Boetius and Wenzhöfer, 2013; Lessard-Pilon et al., 2010; MacDonald et al., 2010; Orcutt et al., 2004). These physical and biological features are supported by diffuse or focused hydrocarbon flow in the upper sediments. The various geological and geophysical indicators reflect not only the presence, but also the intensity, of seepage (Roberts, 2001). A focused advective flux is evidenced by bubble

* Corresponding author at: Department of Geosciences, University of Bremen, Bremen, Germany.
E-mail address: caroline.vl.johansen@gmail.com (C. Johansen).
[1] Present address: Odum School of Ecology, University of Georgia, Athens, GA, USA.

https://doi.org/10.1016/j.epsl.2020.116411
0012-821X/

plumes while diffuse flux is evidenced by the presence of persistent chemosynthetic communities (e.g. bacterial mat coverage).

The flow rates of hydrocarbons through faults and salt-sediment interfaces from the deep source reservoirs to the seafloor can be estimated using seismic data (Macelloni et al., 2012; Simonetti et al., 2013). Below the sediment-water interface, zones of indistinct acoustic return (blanking zones) in subbottom data delineate gas-charged sediments (Abrams, 1992). Depending on the geothermal gradient and sediment pore space, shallow gas hydrates form when sufficiently high fluid flow rates maintain high concentrations of methane in the pore volume near the seawater interface (Haacke et al., 2007). Gas hydrate caps form above the local conduit and promote lateral migration of hydrocarbons around the resulting obstruction (Liu and Flemings, 2006). When hydrocarbon migration continues from below, the gas hydrate caps accrete laterally and vertically, creating mounds that breach the sediment surface (MacDonald et al., 1994). As a result, pathways allowing focused advective flow (hydrocarbon bubble emission) are often present along the edges of gas hydrate mounds (Lapham et al., 2014; Römer et al., 2012).

The western and central Gulf of Mexico (GoM) basin is bounded by a dynamic continental slope where salt tectonism has deformed thick sediment deposits into complex mounds, ridges and basins (Liu and Bryant, 2000), which in turn host prolific natural oil and gas seepage (MacDonald et al., 2015). Hydrocarbon seepage generates extensive authigenic carbonates (Roberts et al., 2010), microbiology and biochemistry (Joye, 2020), benthic communities (Fisher et al., 2007), and may enhance primary productivity of overlying surface waters (D'souza et al., 2016). Persistent seepage of hydrocarbons can be detected via acoustic signatures of bubble plumes in the water column (flares) and video data from bubble release at vents on the seafloor (Römer et al., 2019).

Natural seeps reveal specific locations of large-scale hydrocarbon migration to the seafloor. The fate of hydrocarbons seeping out of reservoirs is regulated by the following processes: 1) Sequestration of hydrocarbons in gas hydrate mound growth; 2) gas hydrate dissolution (e.g. exposed gas hydrate outcrops); 3) focused venting (e.g. bubble streams); 4) diffusive release, or biological consumption (e.g. microbial mediated).

Hydrocarbon seepage results from a complex interplay between reservoirs, pressure regimes, migration pathways, and near surface processes (Abrams, 2005). For a carbon-containing molecule in a deep petroleum reservoir to naturally return to the modern-day carbon cycle, the following series of processes must occur: 1) build-up of overpressure, causing leakage by fracturing the reservoir cap (Clayton and Hay, 1994); 2) upward migration along faults (Leifer and Boles, 2005; Macelloni et al., 2012); and 3) discharge at the sediment-water interface (Johansen et al., 2017; Lapham et al., 2014; Solomon et al., 2008; Wankel et al., 2010). The latest, in particular, generates distinctive signatures (e.g. bubble plumes at the seafloor or surface oil slicks) that can be detected acoustically, and/or visually.

The first objective of this work was to examine the processes that link the different stages of vertical hydrocarbon migration from reservoir to seafloor, and to constrain the fate of all hydrocarbons throughout this journey. We combined diverse data sets, which range from km-scale 3D multichannel seismic data to cm-scale seafloor observations, to systematically describe the different processes involved in hydrocarbon migration and sequestration. To this point, a conclusive methane budget is lacking, despite an abundance of research. Therefore, the second objective was to semi-quantitatively interpret observations and develop a first-order methane budget at this site using a geo-systems approach that could be applied to seeps across the GoM.

2. Site description

The study site, located in outer continental shelf lease block Green Canyon 600 (GC600) is an example of a well-studied mid-slope seep zone with ample satellite data documenting surface oil slicks, seismic/acoustic mapping, and seafloor observations (Garcia-Pineda et al., 2010; MacDonald et al., 2015). The bathymetry of the Northern GoM consists of depressions and ridges formed by salt deformation (Roberts et al., 2010). The ~5 × 5 km lease block GC600 (Fig. 1a) falls on the rising ridge of the salt-driven bathymetry, a feature associated with seepage elsewhere in the GoM (Macelloni et al., 2012; Simonetti et al., 2013; Wilson et al., 2014) (Fig. S.1).

Following the same terminology defined by Leifer and Boles (2005) and Garcia-Pineda et al. (2010), our study was focused in an approximately 2 km diameter seep zone where there are two main mounds with multiple and persistent vents that released gas and oil. Mega Plume and Birthday Candles are the most prominent seep domains containing multiple vents within this seep zone (Wang et al., 2016; Johansen et al., 2017; Krajewski et al., 2018; Mitchell et al., 2018; Diercks et al., 2019; Teske and Joye, 2020) (Fig. 1b). Birthday Candles domain was located to the SE of the salt ridge at a depth of 1215 m. Mega Plume domain was located 1 km NW from Birthday Candles at a depth of 1222 m. On each domain, the vents are comprised of clusters of small pores in gas hydrate outcrops through which multiple streams of oily and non-oily bubbles escape (Johansen et al., 2017). The domains also include many well-developed examples of fluid flow indicators described previously. For a more detailed description of the site seafloor morphology, refer to Diercks et al. (2019) and Mitchell et al. (2018).

3. Methods

We examined the geophysical and geochemical aspects of the system using a broad suite of observations. The different datasets examined during this study are listed in Table 1, and include the following: 1) multichannel seismic data (survey area ~60 × 20 km) to delineate subsurface geology and tectonics; 2) chirp subbottom profiles (survey area 1.2 × 1.8 km) to detect acoustic near bottom blanking zones generated by gas-charged sediments; 3) bathymetry and backscatter (survey area 1.2 × 1.8 km), as well as AUV photogrammetric images (survey area 60 × 60 m) of the seafloor, to map geomorphology; 4) multibeam echosounder returns to detect bubble flares in the water column (survey area ~ 5 km^2); 5) video time lapse cameras (VTLC), ROV, and submersible video to observe bio-geological features on the seafloor (at a cm-scale); and 6) gas chromatography/mass spectrometry (GC/MS) characterizations of oil samples from a reservoir, seafloor vent, and surface oil slick, to fingerprint the oil chemistry at each stage of seepage.

3.1. Deep seismic data

The GC600 deep subsurface geology (hydrocarbon reservoir, salt position, overburden sedimentary sequences) and the faults and fracture pathways were analyzed using 3D multichannel seismic data archived by the Bureau of Ocean Energy Management (BOEM). Geophysical and geological interpretation were carried out using Schlumberger's GeoFrame reservoir characterization software. The seismic data included one pre-stack, time-migrated seismic volume sampled at 4 ms and one full wave equation pre-stack depth migrated volume. Source to seep travel distances were computed utilizing a software-embedded digital planimeter. We present two representative seismic lines extracted from the 3D volumes (Fig. 2, 2c insert). The first one stretches over 60 km in a predominantly

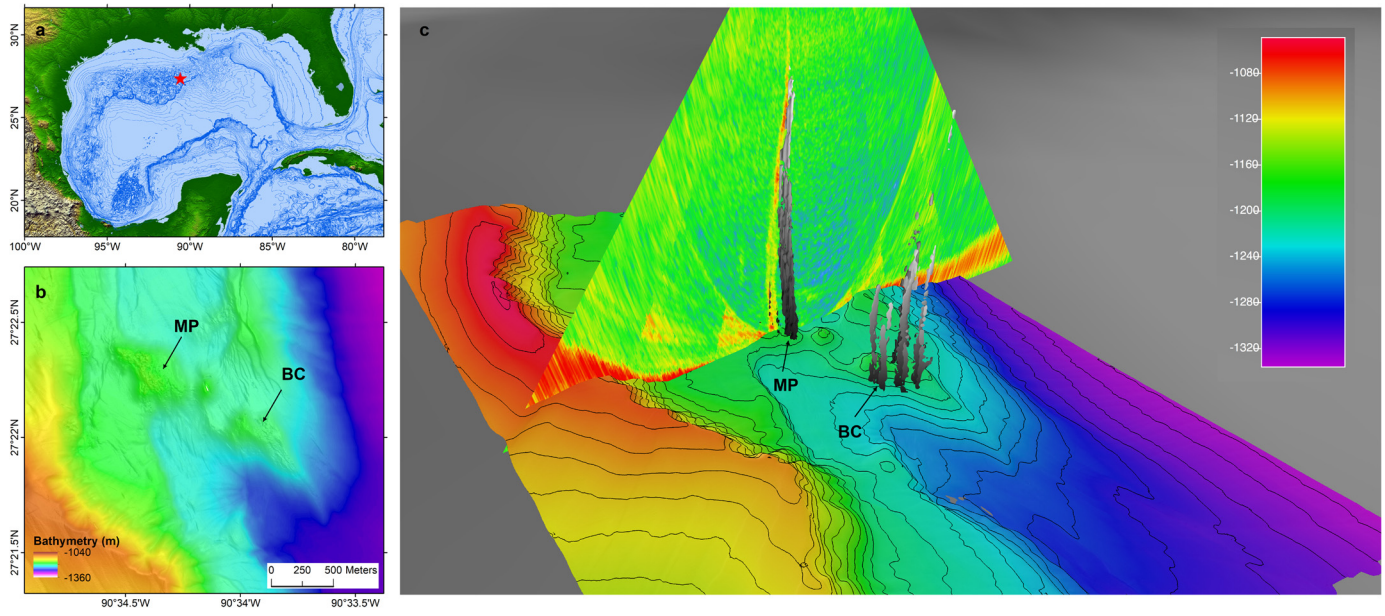

Fig. 1. **a** Study location, Gulf of Mexico, GC600. **b** Shows the two seep domains Mega Plume (MP) and Birthday Candles (BC). The entire seep zone extends over 2 km. **c** 3D rendition of the flares detected at both seep domains MP and BC. (For interpretation of the colors in the figure(s), the reader is referred to the web version of this article.)

Table 1
List of objectives, instruments, and methods used to collect data. DOI for data are listed in acknowledgments.

Objective	Collection type	Instrument	Program
Seafloor observations	Video data	VTLC[a], DSV ALVIN, ROVs	ECOGIG-1, ECOGIG-2
Bubble flares in the water column	Multibeam Echosounder	Kongsberg EM 302, Konsberg EM 122	ECOGIG-1
Seafloor Geomorphology	Photo survey	Mola Mola AUV	ECOGIG-1
Blanking zones and hydrate coverage	Bathymetry, backscatter and subbottom survey	Eagle Ray AUV	ECOGIG-1
Faults and salt distribution	Seismic survey	Q-Marine point-receiver	BOEM seismic archive
Chemical analysis	Manual collection UCGTN[b]	GC/APCI-MS[c]	Deep-C

[a] VTLC: Video Time Lapse Camera.
[b] UCGTN: U.S. Coast Guard certified Teflon collection nets.
[c] GC/APCI-MS: Gas chromatography/atmospheric pressure chemical ionization mass spectrometry.

West-East direction and reaches 20 km deep in the sediments (Fig. 2b). The second one passes directly over the Mega Plume and Birthday Candles domain and traverses approximately 10 km in the North-South direction and is 4 km deep (Fig. 2c).

3.2. AUV-derived chip data

The chirp subbottom profile data covered an area of 5 × 5 km and was acquired using the *AUV Eagle Ray* equipped with a Kongsberg GeoAcoustics subbottom profiler, operating at 5-10 kHz frequency range. A total of 32 subbottom profiles were collected by the AUV flying at a nominal altitude of 25 m from the seafloor. The profiles, extending NW to SE are approximately 1.8 km long, with a spacing of 36 m between lines. Subbottom profile data processing included optimal matched filtering of the sweep pulse and time static correction to compensate for slight fluctuations in the AUV's altitude. Processed subbottom data were depth converted using a constant velocity of 1500 m/s and imported into a single Kingdom® Suite project. Interpretation of the data consists of extensive picking to identify the geological units and acoustic blanking zone anomalies (Løseth et al., 2009) indicating gas-charged sediments. The depth to the top of the gas-charged units was determined manually by selecting both the seafloor reflector and the top of the gas-charged zone, and then subtracting them from each other. These values, which provide the sediment thickness above the gas-charged sediments, were interpolated and gridded with 2 m spacing to map the spatial distribution of the gas-charged blanking zones. (Fig. 3). The blanking zones were delineated in ArcGIS by computing 1 m contours of the map, and manually picking the contour that best fits the extent of the gas blanking (Fig. 3). This contour was used to compute the area of the blanking zone. In order to provide an estimation of the error, 18 m-wide buffers (half of the subbottom line spacing) were delineated on both sides of the blanking zone contour to calculate minimum and maximum areas.

3.3. Multibeam bathymetry and backscatter

The bathymetry and co-registered backscatter data were acquired with the *AUV Eagle Ray* using a Kongsberg EM2000 multibeam echosounder. The bathymetry data were corrected for errors due to navigation, altitude parameters (pitch, roll, heave, and yaw), sound velocity, and tide. Successively the soundings were edited to remove spikes and other artifacts and then gridded at 1 m bin resolution (Fig. 4). Backscatter data underwent a series of corrections following the workflow of Beaudoin et al. (2002) and Clarke et al. (1996). Backscatter intensity is used to infer seafloor sediment characteristics, with photo and video observations serving to ground truth the interpretation.

3.4. Hydroacoustic water column surveys

Midwater ship-borne multibeam surveys were conducted to detect flare anomalies indicative of gas bubbles ascending in the water column (Weber et al., 2012). Data sets from both *R/V Falkor* and expedition F006b (Kongsberg EM302) *R/V Atlantis* expedition AT26

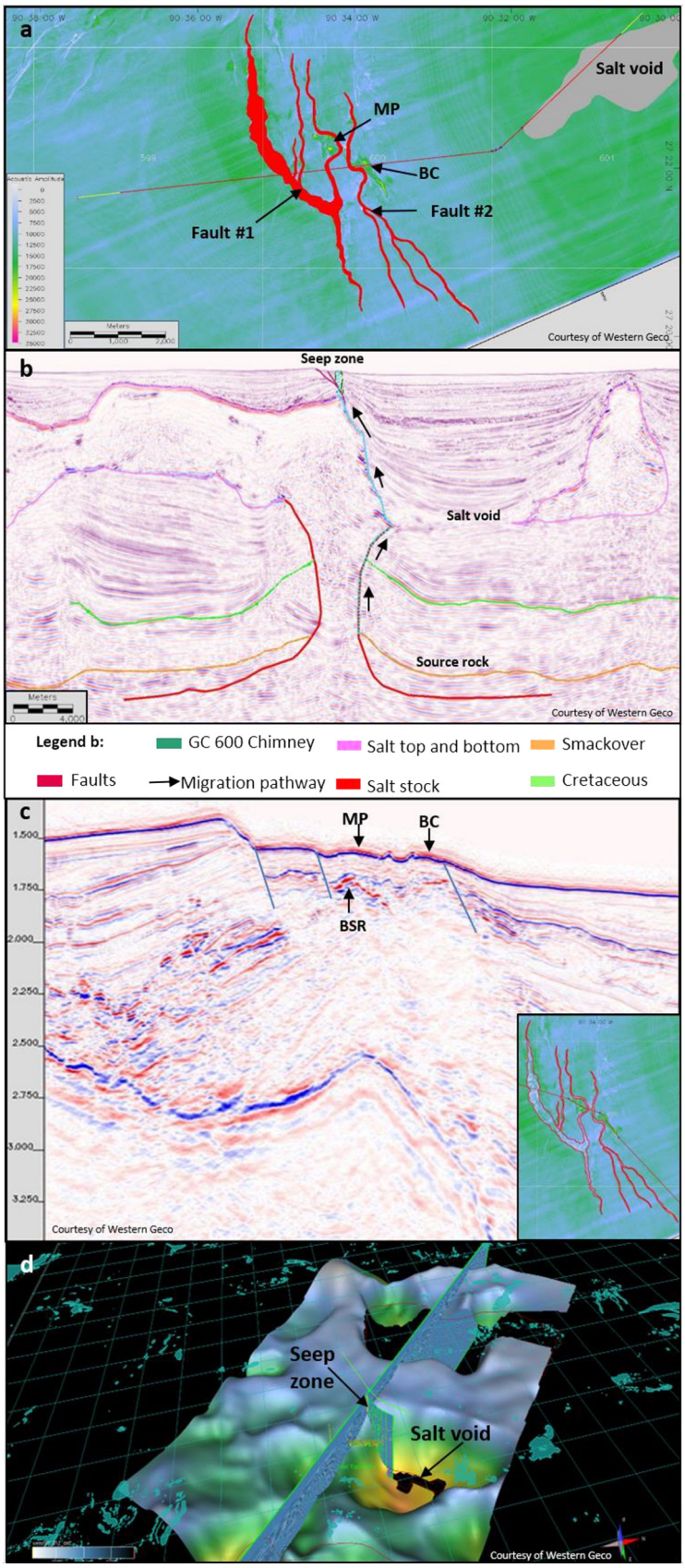

Fig. 2. Geophysical structures in the GC600 region. **a** Seafloor amplitude map. Red line shows seismic traverse for seismic section shown in **b**. Red contours delineate interpreted faults on the seafloor amplitude map. **b** Seismic section of the traverse in **a**. **b** Shows inferred migration pathway of oil and gas from the source rock: Cretaceous (∼11 kmbsf) or Smackover (14 kmbsf). **c** Overview in the time domain. Blue lines show interpreted faults. Discontinuous Bottom Simulating Reflector (BSR) identified at approximately 305 mbsf (vertical access is in two way travel time). Insert shows the traverse of seismic line. **d** Grid of the base of the salt coverage. The salt void is the same as the ones seen in **a** and **b**.

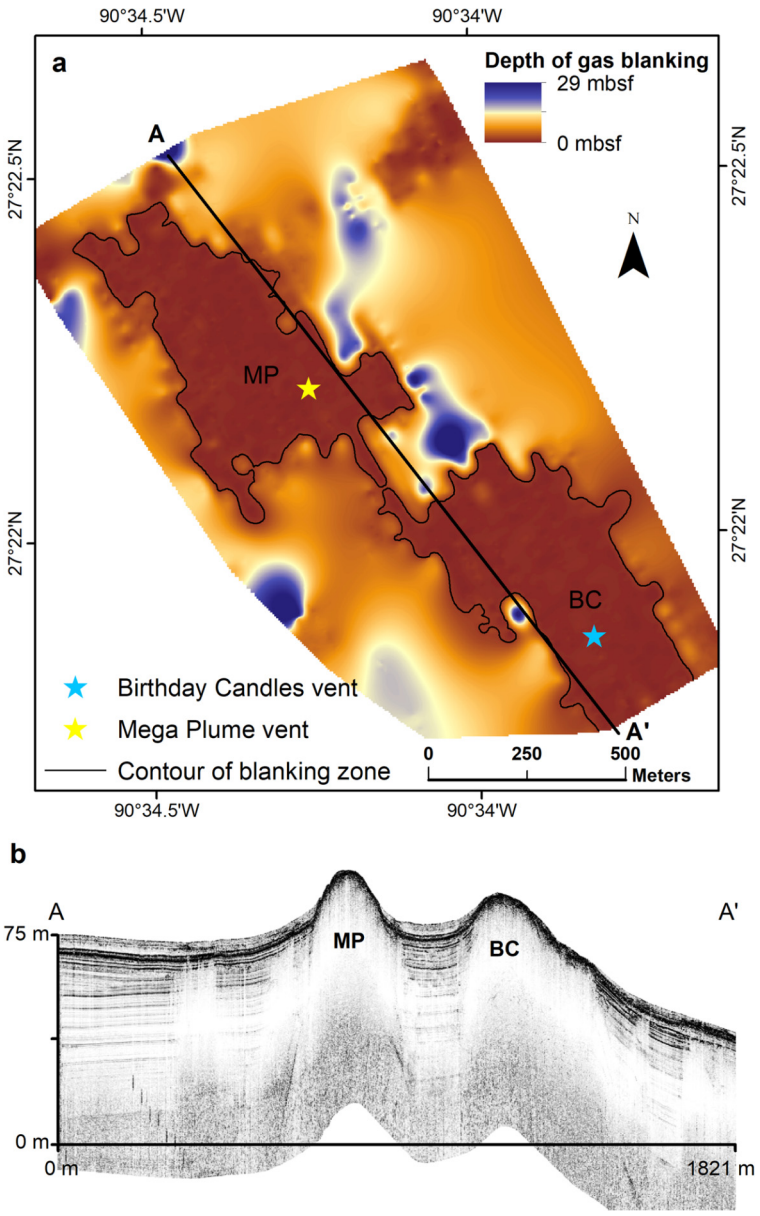

Fig. 3. a Grid showing base of the blanking zone determined with a closed contour of 1 m intervals. **b** Chirp line of corresponding line in **a** (A-A′).

13 (Kongsberg EM211) were analyzed. The horizontal swath coverage was approximately 3.5 km with a combined beam angle of 120° and cell resolution of each beam was 4.1 m. The FMMidWater Toolbox in Fledermaus was used to identify flares and delineate their 3D envelopes (Fig. 1c). Multiple survey lines passed over the seep zone and flare points were manually geo-picked, generating an array of points for each plume detected by the ships multibeam systems. Acoustic flare points were grouped to determine the location of the active plumes following the method by Diercks et al. (2019) (Fig. 4).

3.5. Seafloor imaging systems and measurements

To analyze the geomorphology of the GC600 seep, the *AUV Mola Mola* (Diercks et al., 2009; Woolsey et al., 2015) surveyed a 60 × 60 m area in the Mega Plume domain (Fig. 5a). Agisoft PhotoScan software was used to perform close-range photogrammetry on the acquired images to create a Digital Terrain Model (DTM). Images were obtained at 3 m altitude with a 15% overlap between survey lines. For sections of interest in the survey area, a height field mesh suitable for terrain modeling was built to visualize distinct topographical depressions, reliefs, biology, and detailed color features (Fig. 5b,d). *Mola Mola* did not survey the Birthday Candles domain; therefore, *DSV ALVIN* and VTLC videos (Johansen et al., 2017) were examined for detailed observations and measurements of the seafloor morphology and biology in this area (Fig. 5c,e,f,g).

For each seep domain, the dimensions of the area of bubble release were estimated from VTLC images of an active vent (Johansen et al., 2017). For the methane budget calculations we assume the same size of bubble release areas for the active vents in each seep domain. The total area of bacteria mats was estimated by measuring the coverage of bacterial mats on the *Mola Mola* photomosaic and extrapolating the percent coverage over the entire seep domain. The sizes of brine pools, mussel beds, and gas hydrates were determined by analyzing frame grabs from ALVIN submersible dive videos (dives AL4690, and AL4692). Laser pointers provided a scale on the images, and ImageJ software was used to measure the areas.

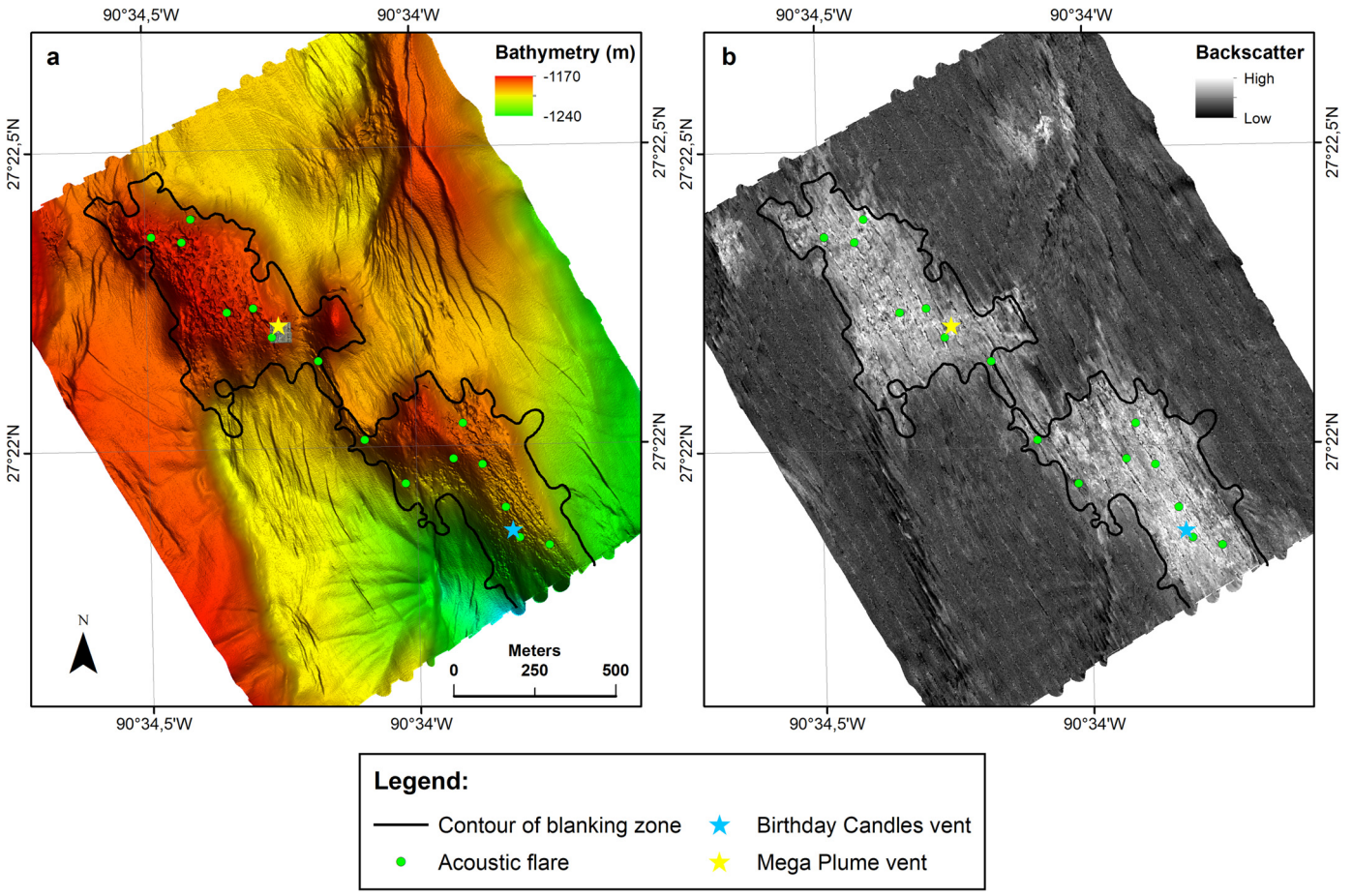

Fig. 4. a Bathymetry of GC600 seep domain (map is vertically exaggerated 6 times to emphasize seafloor morphology). **b** Backscatter data with blanking contour outlined to show match. Mega Plume is the mound to the NW and Birthday Candles is the mound to the SE. Black contour outlines blanking zone in subbottom data. Green points show the locations of the mapped acoustic flares. Stars are positions of individual vents ground-truthed with VTLC records, and AUV and submersible surveys. The small grey square under the yellow star on the bathymetry map represents the extent of the *Mola Mola* photomosaic.

3.6. Chemical data and analysis

Oil samples were collected from surface slicks at Birthday Candles and Mega Plume using U.S. Coast Guard certified Teflon collection nets (UCGTN) attached to extractable poles. To sample the oil containing bubbles released from the seafloor vent at Mega Plume, the UCGTN was attached to a T-handle and maneuvered over the sampled vent using the *Global Explorer ROV* (bubble stream Fig. 5c). The oil covered UCGTNs were stored in a sealed box on the ROV tray during the ascent. On-board the vessel, the UCGTNs were immediately stored in sealed glass jars and frozen at −20 °C. Additional samples of reservoir crude oil were provided from the Holstein Spar oil platform (Anadarko) located approximately 5 km SE from the GC600 seep zone.

The UCGTN oil samples were extracted with toluene (HPLC grade), evaporated under a gentle nitrogen flow for complete solvent removal, and diluted with dicholoromethane (HPLC grade) to a concentration of 20 mg/mL. Crude oil samples (Holstein and Macondo) were subjected to five-fold dilution with the dicholoromethane. A chemical analysis was performed using a gas chromatography/atmospheric pressure chemical ionization mass spectrometer (GC/APCI-MS) (Lobodin et al., 2016).

The diagnostic biomarker ratios were calculated from chromatographic peak areas for the corresponding compounds observed in the oil samples (Fig. 6). Reproducibility of the analytical procedure was confirmed by the triplicate analysis of all samples (10% accuracy). Of the diagnostic ratios Ts/Tm, H29/H30, H31S/H31R, H32S/H32R, H30/(H31+H32+H33+H34+H35), C27$\alpha\beta\beta$/C29$\alpha\beta\beta$ steranes, C27$\beta\alpha$/C29$\beta\alpha$ diasteranes are commonly used for identification, correlation, and differentiation of petroleum samples (Hood et al., 2002; Wang and Stout, 2007) (Fig. S.3).

4. Results and discussion

Seismic, subbottom, bathymetric, and backscatter data were examined to identify hydrocarbon migration pathways from source rock to water column. By overlying the bathymetry and backscatter over blanking zones and comparing these results to seismically interpreted fault positions, we determined migration pathways that are consistent with acoustic flares in the water column. The pathways are also consistent with bubble streams observed with AUV surveys, *DSV ALVIN* flyovers, and VTLC footage. In addition, chemical analysis connects the entire system by establishing that the oil seeping out at the seafloor and reaching the sea surface as slicks, is chemically similar to a crude oil sample from the reservoir (Fig. S.4, S.5).

4.1. Deep seismic analysis

Characterization of the system begins with the analysis of the multichannel seismic data that covers 60 × 20 km (dimensions for seismic overview; horizontal and vertical distance respectively) to provide the overall geological context of the system. The seismic data revealed the presence of a distinct void of approximately 10 km^2 in the salt horizon, creating an opening in the salt layer through which hydrocarbons can migrate upward (Fig. 2a, b, and

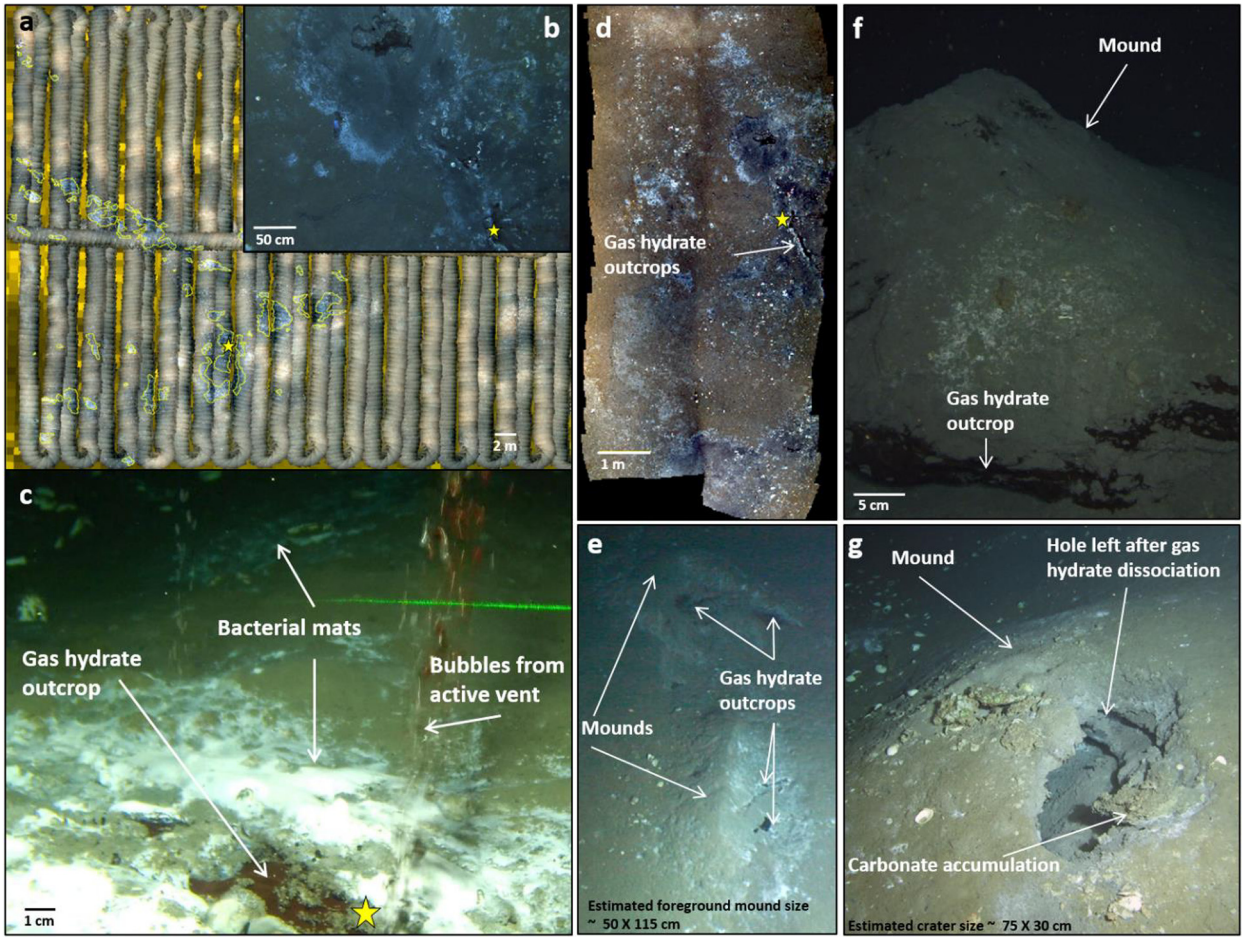

Fig. 5. Seafloor observations at Mega Plume and Birthday Candles. Yellow star is the same vent in each image **a, b, c,** and **d**. **a** 60 × 60 m *Mola Mola AUV* track at Mega Plume. Each survey line is 2 m wide captured from 3 m altitude. Bacterial mats outlined in yellow. **b** Individual image from the *Mola Mola* mosaic (**a**). **c** Frame grab from VTLC. **d** Slice from *Mola Mola* survey. **e** Frame grab from *ALVIN* dive at Birthday Candles. **f** Close up image of a mound at Birthday Candles. **g** Mound showing gas hydrate dissociation leaving a crater of approximately 75 × 30 cm.

d). Fig. 2b highlights the most likely migration pathway for the oil and gas from the source rock, along the salt-sediment interface and then shallow fractures, through to the seep zone. The seismic data do not provide details of an individual reservoir; hence, the migration pathway is described from the source rock: Cretaceous (∼11 kmbsf) or Smackover (14 kmbsf) (Fig. 2b). The amplitude maps (Fig. 2a, 2c insert) delineate the position and trend of the surface faults in relation to the Mega Plume and Birthday Candles seep domains. Additionally, Fig. 2c shows a bottom simulating reflector (BSR) indicating that the seeps are within the gas hydrate stability zone (GHSZ).

Areas of vertical or collapsed salt structures create more effective migration conduits than faults (Hood et al., 2002). Therefore, the interpreted void in the salt canopy creates an opening and effective migration conduit for the fluids from the reservoir to reach the seafloor. Salt related deformation is often transferred to shallow subsurface unconsolidated sediments via a complex network of faults and fractures, which multichannel seismic data cannot resolve. Hence the migration of hydrocarbons above the salt body can be inferred by detailed analysis of chirp subbottom profiles and seafloor bathymetry. The mounds could be caused by the intersection of deep and shallow faults, in particular surficial faults branching in two arms that appear to feed into the two separate seep domains, Birthday Candles and Mega Plume (Fig. 2a Fault #1 and #2).

4.2. Subbottom analysis

The subbottom data revealed the presence of gas-charged sediments in the upper 75 mbsf, particularly below the Birthday Candles and Mega Plume seep domains. This is evidenced by two large blanking zones, indicating free gas. The minimum sediment thickness above the blanking zones was 0.31 m (Fig. 3a-b). The minimum to maximum range of the blanking zone area for Birthday Candles was 2.0×10^5–3.1×10^5 m^2 and 1.9×10^5–3.3×10^5 m^2 for Mega Plume (Fig. 3a, Table 2).

Acoustic anomalies in the subbottom data along with the presence of a large number of seafloor pockmarks suggests that the sediments in this area are gas-charged (Fig. 3b, S2). Heat probe or pore fluid salinity data were not available, therefore the sediment gas saturation or the amount of solid gas hydrate within the blanking zone cannot be calculated. However, it is clearly visible in the bathymetry (Fig. 4a) and video data (Fig. 5a-g) that there is or has been gas hydrate accumulation and growth.

4.3. Backscatter and bathymetry analysis

Backscatter and bathymetric data over a 1.2 × 1.8 km area depicted the geomorphology of the seafloor (Fig. 4). The backscatter depicts high reflectivity over a subset of the survey area that corresponds with the locations of the Birthday Candles and Mega Plume seep domains (Fig. 4a, b). Seep domains are areas where migrated hydrocarbons concentrate, accumulate, and transform lo-

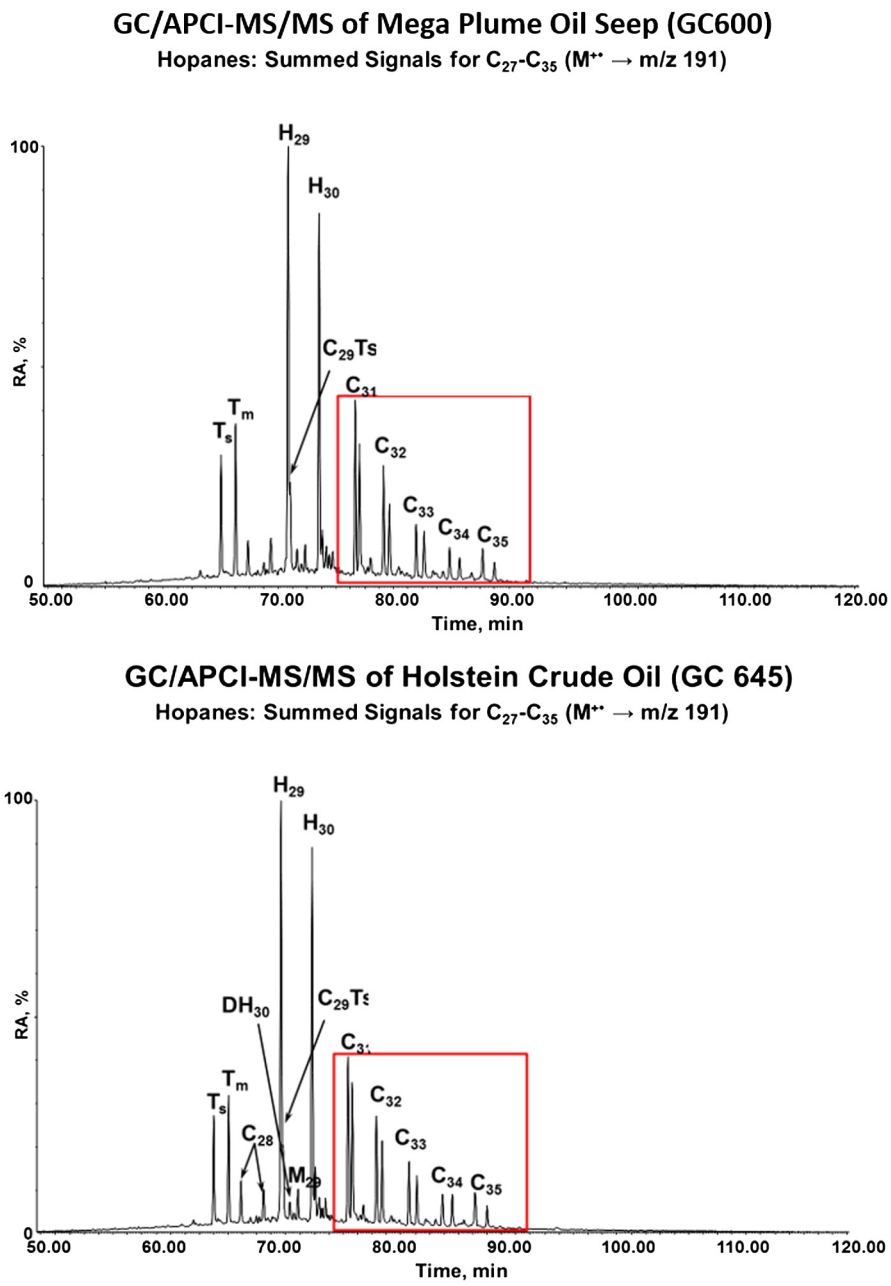

Fig. 6. GC/APCI-MS/MS of an oil sample from the Mega Plume vent, compared to a sample from the Holstein reservoir sample.

cal bathymetry (Fig. 4a). These two mounds, in particular, were characterized by numerous pockmarks (depressions), some up to tens of meters in diameter, indicative of fluid flow possibly via gas hydrate formation and dissolution (Judd and Hovland, 2009; Sultan et al., 2010; Marcon et al., 2014) (Fig. 4a and S.2).

4.4. Hydroacoustic vent detection

The number of vents was based on the number of flares within the closed contour of the blanking zone for each domain (Fig. 4a-b). In total, 8 vents were identified at Birthday Candles and 7 vents at Mega Plume (Fig. 4a-b). All vents occurred on the mounds and coincided with high backscatter areas (Fig. 4). Due to navigation imprecision, the position of the AUV map in relation to the ship-based hydroacoustic flare mapping may be off by 20-50 m. Therefore, the exact location of the vents on the AUV map may be offset by this much. The number of vents within each domain is consistent with results from Diercks et al. (2019) who also used the acoustic survey data sets from *R/V Falkor* (Kongsberg EM 302).

4.5. Seafloor imaging analysis

We used the photomosaic as well as footage from the VTLC to document and estimate the extent of various surficial seepage-related features, such as gas hydrate outcrops, bacterial mats, brine pools and mussel beds. Assessing the areas affected by fluid seepage is crucial to derive methane fluxes for our budget estimation (Table 2). At Mega Plume, gas hydrate outcroppings were mostly visible beneath cracks in the sediments, while large mounds with exposed hydrate deposits could be seen at Birthday Candles. A crack that exposed underlying gas hydrate outcropping at Mega Plume measured approximately 7.5 m long and 0.1 m wide and coincided with an area of active bubble release (Fig. 5d). At Birthday Candles, we observed several mounds where bubbles escaped from patches of gas hydrate (Fig. 5e-f). Based on measurable out-

Table 2
Putative input and output of methane in the system.

	Birthday Candles		Mega Plume	
	Low-end member	*High-end member*	*Low-end member*	*High-end member*
INPUT				
Flux (mol/m^2/yr)[a]	1.42×10^3	7.10×10^3	1.42×10^3	7.10×10^3
Blanking area (m^2)[f]	1.98×10^5	3.09×10^5	1.87×10^5	3.26×10^5
Input (mol/yr)	2.81×10^8	2.20×10^9	2.66×10^8	2.31×10^9
OUTPUT				
Bubbles				
Flux (mol/m^2/yr)[b]	1.51×10^6	5.82×10^6	9.69×10^7	1.60×10^8
Total vent area (m^2)[f]	9.60×10^{-2}	9.60×10^{-2}	3.08×10^{-2}	3.08×10^{-2}
Output (mol/yr)	1.45×10^5	5.59×10^5	2.99×10^6	4.93×10^6
Diffusive				
Flux (mol/m^2/yr)[c]	29.0	29.0	29.0	29.0
Total Bac. Mat area (m^2)[f]	5.72×10^3	8.94×10^3	5.40×10^3	9.41×10^3
Output (mol/yr)	1.66×10^5	2.59×10^5	1.57×10^5	2.73×10^5
Dissociative				
Flux (mol/m^2/yr)[d]	785	785	785	785
Total GH outcrop area (m^2)[f]	6.00	6.00	5.25	5.25
Output (mol/yr)	4.71×10^3	4.71×10^3	4.12×10^3	4.12×10^3
Miscellaneous				
Brine pool (mol/m^2/yr)[e]	0.90	1.30	0.90	1.30
Brine pool area (m^2)[f]	0.36	9.98	0.36	9.98
Output (mol/yr)	0.32	13.0	0.32	13.0
Mussel bed (mol/m^2/yr)[c]	0.89	0.89	0.89	0.89
Mussel bed area (m^2)[f]	2.81×10^{-2}	0.16	2.81×10^{-2}	0.16
Output (mol/yr)	2.50×10^{-2}	0.15	2.50×10^{-2}	0.15
TOTAL OUTPUT (mol/yr)	3.15×10^5	8.23×10^5	3.15×10^6	5.21×10^6
INPUT - OUTPUT (mol/yr)	2.81×10^8	2.20×10^9	2.62×10^8	2.31×10^9
Max. possible hydrate growth				
GH vol. growth (m^3/yr)	3.76×10^4	2.94×10^5	3.51×10^4	3.08×10^5
GH growth rate (m^2/yr)	19.0	94.9	18.8	94.7

[a] Smith et al., 2014, [b] Johansen et al., 2017, [c] Solomon et al., 2008, [d] Lapham et al., 2014, [e] Wankel et al., 2010, [f] This paper.
GH: Gas Hydrate.

crops, we approximate the area of hydrate outcrops to be 0.75 m^2 around each vent. If we assume, for the sake of our budget estimations, that all vents of each seep domain have similar dimensions and features, the total area of gas hydrate outcrops would be 6.0 m^2 at Birthday Candles, and 5.3 m^2 at Mega Plume based on the number of vents in each seep domain.

The measurable vent size was 120 cm^2 at Birthday Candles and 44 cm^2 at Mega Plume. Extrapolating this to the entire seep domain by multiplying with the number of active vents on each seep domain produced a total vent area of 0.1 m^2 at Birthday Candles domain, and 0.03 m^2 at Mega Plume domain. The total area of bacterial mat coverage in the *Mola Mola* photo survey was 104 m^2, which corresponds to 2.9% coverage of the survey area. Assuming the bacterial mat ratio is consistent over entire seep domain, the range of minimum and maximum area of bacteria mat coverage is 5.7×10^3–8.9×10^3 m^2 at the Birthday Candles domain, and 5.4×10^3–9.4×10^3 m^2 in the Mega Plume domain (Table 2). Diffusive flux indicated by bacterial mats can often be found tens of meters from focused vents, and therefore it is likely that bacterial mats existing outside the survey area have been missed. Larger scale *AUV* photo surveys and repeated surveys would be necessary to analyze the spatial distribution and temporal variability of these sites in order to improve these coverage estimates.

The measured areas at brine flows and mussel beds are based on the measurements of two brine pools and two mussel beds that were observed with the ALVIN submersible. The estimated areas are 0.4 and 10 m^2 for the brine pools, and 0.03 and 0.16 m^2 for the mussel beds (Table 2). These values are not representative of the total density of brine pools and mussel beds in the seep domain and are negligible for the methane budget presented in this paper. We incorporated them to address and identify that they are part of a biological filter and to underscore the need for more information on their size, and distribution patterns at seeps. However, a better understanding of their distribution within the seep domains would be necessary to constrain the effect of these particular features on the budget. Currently, there is insufficient data to determine the coverage of these values in the seep domains, therefore, the output of these individual processes is only reported (Table 2).

4.6. Methane input and output

Once the overall geological system and structural architecture has been set, we quantify the overall methane budget by combining our measured areas to published values of methane fluxes (Smith et al., 2014; Johansen et al., 2017; Solomon et al., 2008; Lapham et al., 2014; Wankel et al., 2010), Table 2. The system is defined as the movement of methane throughout each seep domain (Mega Plume and Birthday Candles) (Figs. 1b, 4), starting with the input of methane from the top of the salt ridge to the seafloor, and ending with the processes of methane "removal" (output) at the seafloor/water column interface. These processes at the seafloor/water column interface are divided into different categories: focused, diffusive, and dissociative. The input value is compared to the output and the difference between the two is referred to as the "missing methane." The "missing methane" is either methane that has not been accounted for, or methane that is left in the system (e.g. underestimation of biological consumption, or methane saturated in the sediments). This approach creates a

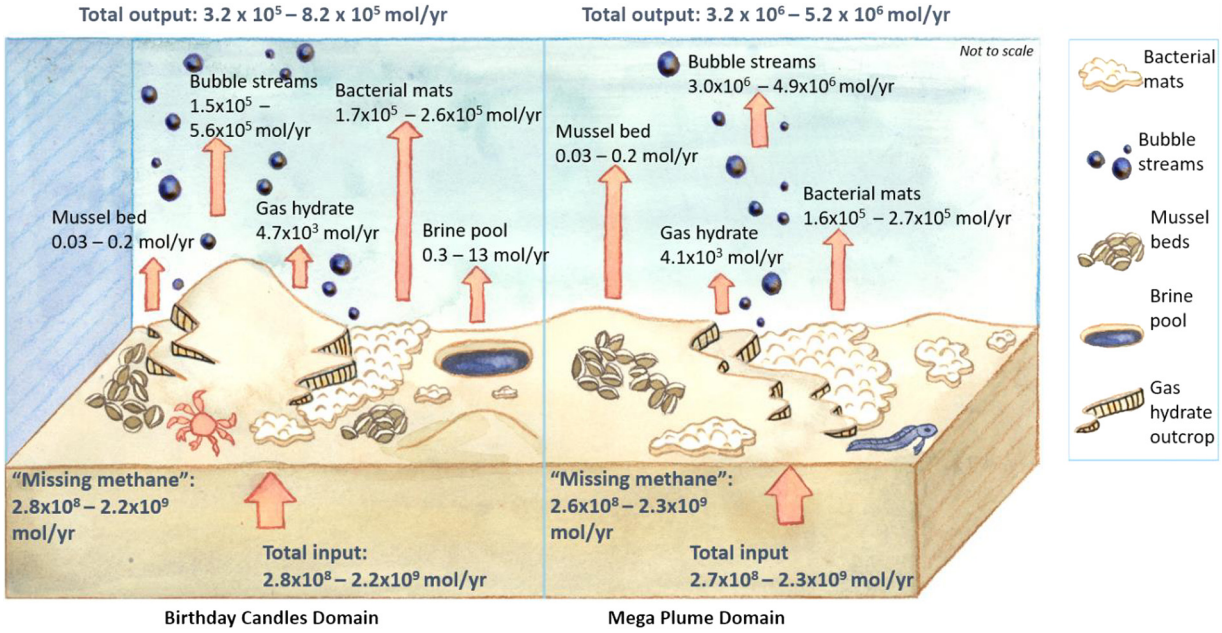

Fig. 7. Schematic of the methane input and output at both Birthday Candles and Mega Plume. Values from Table 2.

basis for further research by holistically incorporating aspects of the seep system and delineating areas where more in-depth studies are necessary. Fig. 7 depicts the estimated methane input and output through all considered categories.

4.6.1. Input

The input represents the amount of methane coming into the system from the top of the salt ridge approximately 2 kmbsf (Fig. 2b). To determine this, the flux of methane from the top of the salt ridge is considered because between this point and the seafloor there is enough fracturing in the sediments to assume hydrostatic pressure (Mann and Mackenzie, 1990). Smith et al. (2014) present a two-phase solute and heat advection-diffusion model to estimate the methane flux from the salt edge to the seafloor at two different seep sites in the GoM, MC852/853, and GB425, located approximately 165 km NE, and approximately 195 km NW from GC600 respectively. Unfortunately, this type of model has not been performed at GC600 and does not account for the biodegradation of methane from the salt ridge to seafloor. However, the values estimated by Smith et al. (2014) at MC852/853 are considered the most relevant for an estimation of methane influx from depth at GC600 based on the following similarities between GC600 and MC852/853:

- similar seafloor temperature (MC852/853: 5 °C, GC600: 4.5 °C)
- persistent oil slicks at the sea surface
- presence of a salt body at the same stratigraphic level
- blanking zones in the shallow sediments
- a clear and visible BSR
- bathymetry of venting area that is mounded (elevated topography), and roughly circular
- active oil seepage
- carbonate hard grounds and chemosynthetic communities

If we consider the flux values calculated by Smith et al. (2014) and multiply it with the measured areas of the contoured blanking zones at Birthday Candles and Mega Plume (Fig. 4), the resulting inputs of methane in the system are 2.8×10^8–2.2×10^9 mol/yr at Birthday Candles, and 2.7×10^8–2.3×10^9 mol/yr at Mega Plume (Table 2).

The values of hydrocarbon flux estimates by Smith et al. (2014) are 3 orders of magnitude higher than previous studies (Leifer and MacDonald, 2003; Milkov et al., 2003). One of the reasons for this, among others, is the fact that this study records the long-term flux over the entire seep domain which has not been accomplished in the other studies (refer to Smith et al., 2014 for detailed description). Although this model has margins of error that may result in overestimations of gas flux (Rooze et al., 2020), it is the only one that encompasses an entire seep domain in a setting similar to that of GC600. In general, to improve the accuracy of models, more field observations and the coupling of models with direct in situ measurements are needed (Smith et al., 2014; Rooze et al., 2020).

4.6.2. Output categories

The "focused output" category considers methane release from vents. A vent is composed of a cluster of pore openings extruding from gas hydrate outcrops, through which methane containing bubbles escape (Johansen et al., 2017). The larger the vent, the more pore openings for bubble release. The flux of methane released in the form of bubbles was quantified using the time series video analysis of bubble release (Johansen et al., 2017). To calculate the focused output, we combined the range of bubble flux values calculated by Johansen et al. (2017) at two different vents within the Mega Plume seep domain and two separate vents at the Birthday Candles seep domain with the measured area of a vent (Fig. 5). These values were then multiplied by the number of active plumes in each seep domain (Fig. 4), providing a range of methane released in the form of bubbles (focused output) between 1.5×10^5–5.6×10^5 mol/yr at Birthday Candles and 3.0×10^6–5.0×10^6 mol/yr at Mega Plume (Table 2).

These focused output values assume that the bubble release is pure methane, which is not fully representative of this site, as it is notorious for its natural oil release (Johansen et al., 2017; Garcia-Pineda et al., 2010; MacDonald et al., 2015; Diercks et al., 2019; Joye, 2020). The sampled vents include a mixture of oil coated and non-oil coated bubbles. Generally more oil containing bubbles were observed at Birthday Candles than at Mega Plume (Johansen et al., 2017). This causes the estimated methane output from bubble release to be an overestimation by a factor of approximately 5 (Johansen et al., 2017).

Methane consumption of bacterial mats were used as an indicator for diffuse flux of methane out of the system. However, as diffusive flux also occurs in sediments where bacterial mats are not visibly present these values are likely a gross underestimation. To determine preliminary values for the methane flux across the seafloor at bacterial mats, the values of methane flux calculated using the MOSQUITO system by Solomon et al. (2008) was used. MOSQUITO is an osmotic pump that uses a tracer injection device to measure fluid flow rates and solute fluxes at approximately 20-26 cmbsf. Applying the diffusive flux values of methane at bacterial mats in conjunction with the measured area of bacterial mats, an estimated diffuse methane output of 1.7×10^5–2.6×10^5 mol/yr at Birthday Candles and 1.6×10^5–2.7×10^5 mol/yr at Mega Plume was calculated (Table 2).

Bowles et al. (2019) studied the anaerobic oxidation of methane (AOM) for the first time in quasi situ conditions and found that values of AOM rates at seeps may in fact be up to 100 times higher than previously thought. In areas of high methane concentration, like GC600, the AOM and (sulfate reduction) SR can be decoupled that allows for the possibility of remarkably higher AOM rates than previously measured (Bowles et al., 2019). Additionally bacteria mats only consume a fraction of the methane that reaches them, and therefore are possibly underestimated by a factor of 1-2 (Sommer et al., 2006). This bolsters the idea that the biological communities play a much larger global role in the sequestration/modulation of hydrocarbons entering the hydrosphere than we are able to constrain.

Passive dissociation of gas hydrate occurs when gas hydrate is not covered in sediments and is exposed to the water column (Lapham et al., 2014), leading to benthic exchange of methane. The flux was estimated based on the gas hydrate dissolution rates in similar conditions reported by Lapham et al. (2014). Following Eq. (10) in Lapham et al. (2014) (assuming 80% methane saturation for solid gas hydrate) and a dissolution rate of 15 cm/yr, with the measured hydrate outcrops at both seep sites, a dissociative output of 4.7×10^3 and 4.1×10^3 mol/yr for Birthday Candles and Mega Plume was calculated (Table 2).

Finally, benthic hydrocarbon exchange at brine flows and mussel beds are potentially significant fluxes, but we do not have sufficient data to fully constrain their distribution and fluxes within each seep domain. Estimates of methane flux across the seafloor at mussel beds were based on measurements using the MOSQUITO (Solomon et al., 2008). At brine flows, methane flux from the brine was determined using in situ mass spectrometry (Wankel et al., 2010). In situ methane concentrations were calculated at different depths within the brine fluid (5, 20, and 80 cm) and the estimated diffusive flux was 0.9 – 1.3 mol/m^2/yr, indicating that a very large component of the methane flux escaped both aerobic and anaerobic oxidation (Wankel et al., 2010). While the available information coupled with measurements from this study suggests that their effect is small, with totals of 0.3 – 13 mol/yr for brine pools and 0.03 – 0.1 mol/yr for mussel beds (Table 2), further research is required to determine more precise flux regimes in these habitats.

4.7. Chemical analysis

As recommended by the Nordtest (Faksness et al., 2002), we calculated a correlation coefficient – a quantitative statistical parameter that is used to "fingerprint" the oil — to evaluate matches between the samples. We found that the correlation coefficient based on the biomarker ratios (Ts/Tm, H_{29}/H_{30}, H_{31S}/H_{31R}, H_{32S}/H_{32R}, $H_{30}/\Sigma(H_{31}\text{-}H_{35})$, $C_{27}\alpha\beta\beta/C_{29}\alpha\beta\beta$ steranes, and $C_{27}\beta\alpha/C_{29}\beta\alpha$ diasteranes) for all samples were statistically significant at the 95% confidence level, except the Macondo crude oil (NIST2779) (S.3, S.4). This indicates that the oil seeping out at the seafloor and reaching the sea surface as slicks is geochemically similar to that of the Holstein crude oil (Fig. 6 and S.5).

The GC600 hydrocarbon system is derived from the Upper Jurassic (Tithonian) source rock (Hood et al., 2002). The results of the geochemical signatures of the oil samples collected were diagnostically similar, which agrees with the published data of GoM oil families (Cole et al., 2001; Hood et al., 2002). The exact reservoir that is feeding the GC600 seep zone could not be identified, however, a relationship between biomarkers from oil collected at a vent and a reservoir sample (Fig. 6) that match Tithonian oil family biomarker distributions and not the other oil families in the GoM (i.e. Macondo oil S.4, S.5), could be confirmed. This supports the seismic-based interpretation of the migration path of hydrocarbons from source rock to seafloor (Fig. 2b).

4.8. Methane budget considerations

The overall methane budget is estimated by the summation of the input/output processes described in section 4.6. Our results suggest that the output of the system is 2-4 orders of magnitude smaller than the total input (Fig. 7, Table 2). In section 4.6.1 it is explained that the input values were found to be up to 3 orders of magnitude higher than previous studies (Smith et al., 2014; Rooze et al., 2020). The intricacies of the models used are beyond the scope of this paper; however, if we suppose that input values might be up to 3 orders of magnitude lower, the output values would generally exceed, or fall within the same order of magnitude at Birthday Candles, whereas the output at Mega Plume would always exceed the input. Our output values are likely to underestimate the actual output because of limited data, especially regarding diffuse seepage (i.e. mussel beds, brine pools, gas hydrate dissociation), and assumptions (i.e. visible bacteria mats representing all diffusive flux, bubble release considered only methane). With these considerations, the results of the output in this study and the dimensions of the blanking zones support the calculation of a higher input than previously estimated. This result highlights the data gaps and the need to comprehensively constrain input and output values.

Another implication to consider is that the input value may not be constant over time. Pockmarks in the mounded bathymetry (Fig. 4a, S.2), and observations at the seafloor (Fig. 5g) indicate the growth and dissociation of shallow gas hydrate mounds. Lapham et al. (2010) described the "push-up-pop" model which postulates that shallow gas hydrates remain stable by dissolving at exposed surfaces at the same rate as they formed within subsurface sediments. Assuming there is a sufficient input of methane and the output does not exceed the source, then the mounds seen in Fig. 5f are quite stable. If the dissolution of the exposed gas hydrate continues without a continuous influx, the gas hydrate will dissociate and leave a hole with carbonate edges as seen in Fig. 5g. This process may explain the numerous pockmarks observed in the bathymetry (Fig. 4a and S.2). However, with these data we cannot constrain the time scale of these processes.

Additionally, the amount of subsurface gas hydrate buildup could not be accounted for. If all the "missing methane" within the system were converted to gas hydrate, the rate of gas hydrate volume increase would reach 3.8×10^4–2.9×10^5 m^3/yr at the Birthday Candles domain and 3.5×10^4–3.1×10^5 m^3/yr at the Mega Plume domain (Table 2). This exercise corresponds to a vertical expansion of 19 – 95 cm/yr at both domains. Based on long term observations of the seafloor geomorphology (video footage with ROV, submersible, AUV surveys) at this site, and considering gas hydrate accumulation can be intermittent within the hydrate stability zone from the BSR (approximately 305 mbsf, Fig. 2c) to seafloor (Ruppel et al., 2005); the lower end of this hydrate

expansion range is a plausible explanation of how this "missing methane" could be accounted for.

The deep sea ecosystem can be considered one of the most important players of hydrocarbon cycles at the global scale. In this work, the contribution of biological consumption is considerably underestimated. The complex dynamics of biological consumption in the deep sea cannot be resolved with the limited video data. Seeps are no longer viewed as isolated areas, but important aspects to the overarching deep sea ecosystem (Levin et al., 2016). The interaction of the chemosynthetic communities at seep zones affect the evolution of the ecosystems on the seafloor, water column, and global geochemical cycles (Boetius and Wenzhöfer, 2013).

5. Conclusion

The input of hydrocarbons at the sediment-water column interface manipulates the geomorphology and biology of the system, creating unique ecosystems of checks and balances. By combining the different data sets available at the GC600 seep site, we attempted to identify the different categories of methane output and developed a methane budget that accounts for the incoming methane flux. There was a clear disconnect between the total input and total output (Table 2), leaving a "missing hydrocarbon" value of 2.6×10^8–2.3×10^9 mol/yr. We posit that some of this is used for gas hydrate accumulation and that we are likely significantly underestimating the biological consumption component of this methane budget.

Even with the stated assumptions and points of limited data, we have created a starting point to constrain quantitative measurements which further studies can use as a base line to fill data gaps. This is the first work of its kind in the GoM where we have had such a unique opportunity to combine a variety of data sets of different scales and resolutions ranging across multiple disciplines. With these data we have presented a semi-quantitative interpretation of observations and described the connections between datasets. These connections permit a holistic systems approach for describing natural dynamics within a specific seep system, and can be used as an exemplary springboard for further research.

Declaration of competing interest

The authors declare that they have no known competing financial interests or personal relationships that could have appeared to influence the work reported in this paper.

Acknowledgements

This work was made possible by the support from Ecosystem Impacts of Oil and Gas in the Gulf (ECOGIG) to SBJ under The Gulf of Mexico Research Initiative, the National Science Foundation [awards OCE-1558916 and OCE-1151698 to FJS], and NOAA's National Center for Coastal Oceans Research to NNR. This research was also made possible in part by a grant from The Gulf of Mexico Research Initiative to support the "Ecosystem Impacts of Oil and Gas in the Gulf" (ECOGIG) and Deep-C consortium, and in part by National Science Foundation Award [EF-0801741 and DMR-11-57490]. Data are publicly available through the Gulf of Mexico Research Initiative Information & Data Cooperative (GRIIDC) at https://data.gulfresearchinitiative.org (doi: 10.7266/N7VM49B3, doi: 10.7266/N72V2D45, doi: 10.7266/N7Z31WP7, doi: 10.7266/N7M906N3, doi: 10.7266/N7M906N3). We thank ship mates and the crew members aboard the *R/V Falkor, R/V Pelican, R/V Atlantis* and *E/V Nautilus* for their support and help with data collection. Ship time and ROV use during F006b was provided by the Schmidt Ocean Institute. Additionally we would like to thank Christof Meile and Jurjen Rooze for discussion and comments on this manuscript, Basil Blake for the artistic rendition of the methane budget (Fig. 7), Logan Krajewski for help of chemical analysis in the lab, and Yann Marcon and three anonymous reviewers for their constructive criticism of the manuscript. This is ECOGIG contribution number 443.

Appendix A. Supplementary material

Supplementary material related to this article can be found online at https://doi.org/10.1016/j.epsl.2020.116411.

References

Abrams, M.A., 1992. Geophysical and geochemical evidence for subsurface hydrocarbon leakage in the Bering Sea, Alaska. Mar. Pet. Geol. 9, 208–221.
Abrams, M.A., 2005. Significance of hydrocarbon seepage relative to petroleum generation and entrapment. Mar. Pet. Geol. 22, 457–477.
Beaudoin, J., Hughes Clarke, J., Van Den Ameele, E., Gardner, J.V., 2002. Geometric and radiometric correction of multibeam backscatter derived from Reson 8101 systems. In: Canadian Hydrographic Conference, p. 242.
Boetius, A., Wenzhöfer, F., 2013. Seafloor oxygen consumption fuelled by methane from cold seeps. Nat. Geosci. 6, 725–734.
Bowles, M.W., Samarkin, V.A., Hunter, K.S., Finke, N., Teske, A.P., Girguis, P.R., Joye, S.B., 2019. Remarkable capacity for anaerobic oxidation of methane at high methane concentration. Geophys. Res. Lett.
Clarke, J.E.H., Mayer, L.A., Wells, D.E., 1996. Shallow-water imaging multibeam sonars: a new tool for investigating seafloor processes in the coastal zone and on the continental shelf. Mar. Geophys. Res. 18, 607–629.
Clayton, C., Hay, S., 1994. Gas migration mechanisms from accumulation to surface. Bull. Geol. Soc. Den. 41, 12–23.
Cole, G., Yu, A., Peel, F., Taylor, C., Requejo, R., DeVay, J., Brooks, J., Bernard, B., Zumberge, J., Brown, S., 2001. The deepwater GOM petroleum system: insights from piston coring seepage versus anomalies versus background. In: Gulf Coast Society of Economic Paleontologists and Mineralogists Research Conference, pp. 315–342.
Diercks, A., Asper, V., Williams, J., Woolsey, M., 2009. Advanced technology in motion: NIUST's AUV fleet. In: OCEANS 2009, MTS/IEEE Biloxi-Marine Technology for Our Future: Global and Local Challenges. IEEE, pp. 1–5.
Diercks, A., Macelloni, L., D'Emidio, M., Lucker, S., Woolsey, A., Woolsey, M., 2019. High-resolution seismo-acoustic characterization of Green Canyon 600, a perennial hydrocarbon seep in Gulf of Mexico deep water. Mar. Geophys. Res., 1–14.
D'souza, N.A., Subramaniam, A., Juhl, A.R., Hafez, M., Chekalyuk, A., Phan, S., Yan, B., MacDonald, I.R., Weber, S.C., Montoya, J.P., 2016. Elevated surface chlorophyll associated with natural oil seeps in the Gulf of Mexico. Nat. Geosci. 9, 215–218.
Faksness, L.-G., Weiss, H.M., Daling, P.S., 2002. Revision of the Nordtest Methodology for Oil Spill Identification. SINTEF Report STF66 A 2028.
Fisher, C.R., Roberts, H.H., Cordes, E.E., Bernard, B., 2007. Cold seeps and associated communities of the Gulf of Mexico. Oceanography 20, 118–129.
Garcia-Pineda, O., MacDonald, I., Zimmer, B., Shedd, B., Roberts, H., 2010. Remote-sensing evaluation of geophysical anomaly sites in the outer continental slope, northern Gulf of Mexico. Deep-Sea Res., Part 2, Top. Stud. Oceanogr. 57, 1859–1869.
Haacke, R.R., Westbrook, G.K., Hyndman, R.D., 2007. Gas hydrate, fluid flow and free gas: formation of the bottom-simulating reflector. Earth Planet. Sci. Lett. 261, 407–420.
Hood, K.C., Wenger, L., Gross, O., Harrison, S., 2002. Hydrocarbon systems analysis of the northern Gulf of Mexico: delineation of hydrocarbon migration pathways using seeps and seismic imaging. Surface exploration case histories: applications of geochemistry, magnetics, and remote sensing. In: AAPG Studies in Geology, vol. 48, pp. 25–40.
Johansen, C., Todd, A.C., MacDonald, I.R., 2017. Time series video analysis of bubble release processes at natural hydrocarbon seeps in the northern Gulf of Mexico. Mar. Pet. Geol. 82, 21–34.
Joye, S.B., 2020. The geology and biogeochemistry of hydrocarbon seeps. Annu. Rev. Earth Planet. Sci. 48 (1), 205–231. https://doi.org/10.1146/annurev-earth-063016-020052.
Judd, A., Hovland, M., 2009. Seabed Fluid Flow: The Impact on Geology, Biology and the Marine Environment. Cambridge University Press.
Krajewski, L.C., Lobodin, V.V., Johansen, C., Bartges, T.E., Maksimova, E.V., MacDonald, I.R., Marshall, A.G., 2018. Linking natural oil seeps from the Gulf of Mexico to their origin by use of Fourier transform ion cyclotron resonance mass spectrometry. Environ. Sci. Technol. 52 (3), 1365–1374.
Lapham, L.L., Chanton, J.P., Chapman, R., Martens, C.S., 2010. Methane undersaturated fluids in deep-sea sediments: implications for gas hydrate stability and rates of dissolution. Earth Planet. Sci. Lett. 298, 275–285.
Lapham, L.L., Wilson, R.M., MacDonald, I.R., Chanton, J.P., 2014. Gas hydrate dissolution rates quantified with laboratory and seafloor experiments. Geochim. Cosmochim. Acta 125, 492–503.

Leifer, I., Boles, J., 2005. Measurement of marine hydrocarbon seep flow through fractured rock and unconsolidated sediment. Mar. Pet. Geol. 22, 551–568.
Leifer, I., MacDonald, I., 2003. Dynamics of the gas flux from shallow gas hydrate deposits: interaction between oily hydrate bubbles and the oceanic environment. Earth Planet. Sci. Lett. 210 (3–4), 411–424.
Lessard-Pilon, S., Porter, M.D., Cordes, E.E., MacDonald, I., Fisher, C.R., 2010. Community composition and temporal change at deep Gulf of Mexico cold seeps. Deep-Sea Res., Part 2, Top. Stud. Oceanogr. 57, 1891–1903.
Levin, L., Baco, A., Bowden, D., Colaco, A., Cordes, E., Cunha, M., Demopoulos, A., Gobin, J., Grupe, B., Le, J., 2016. Hydrothermal vents and methane seeps: rethinking the sphere of influence. Front. Mar. Sci. 3, 72.
Liu, J.Y., Bryant, W.R., 2000. Seafloor morphology and sediment paths of the northern Gulf of Mexico deep water. Transactions 45, 95–101.
Liu, X., Flemings, P.B., 2006. Passing gas through the hydrate stability zone at southern Hydrate Ridge, offshore Oregon. Earth Planet. Sci. Lett. 241, 211–226.
Lobodin, V.V., Maksimova, E., Rodgers, R.P., 2016. Gas chromatography/atmospheric pressure chemical ionization tandem mass spectrometry for fingerprinting the Macondo Oil Spill. Anal. Chem. 88, 6914–6922.
Løseth, H., Gading, M., Wensaas, L., 2009. Hydrocarbon leakage interpreted on seismic data. Mar. Pet. Geol. 26 (7), 1304–1319.
MacDonald, I.R., Garcia-Pineda, O., Beet, A., Daneshgar Asl, S., Feng, L., Graettinger, G., French-McCay, D., Holmes, J., Hu, C., Huffer, F., Leifer, I., Muller-Karger, F., Solow, A., Silva, M., Swayze, G., 2015. Natural and unnatural oil slicks in the Gulf of Mexico. J. Geophys. Res., Oceans 120, 8364–8380.
MacDonald, I.R., Guinasso, N.L., Sassen, R., Brooks, J.M., Lee, L., Scott, K.T., 1994. Gas hydrate that breaches the sea floor on the continental slope of the Gulf of Mexico. Geology 22, 699–702.
MacDonald, I.R., Smith, M., Huffer, F.W., 2010. Community structure comparisons of lower slope hydrocarbon seeps, northern Gulf of Mexico. Deep-Sea Res., Part 2, Top. Stud. Oceanogr. 57, 1904–1915.
Macelloni, L., Simonetti, A., Knapp, J.H., Knapp, C.C., Lutken, C.B., Lapham, L.L., 2012. Multiple resolution seismic imaging of a shallow hydrocarbon plumbing system, Woolsey Mound, Northern Gulf of Mexico. Mar. Pet. Geol. 38, 128–142.
Mann, D.M., Mackenzie, A.S., 1990. Prediction of pore fluid pressures in sedimentary basins. Mar. Pet. Geol. 7, 55–65.
Marcon, Y., Ondréas, H., Sahling, H., Bohrmann, G., Olu, K., 2014. Fluid flow regimes and growth of a giant pockmark. Geology 42 (1), 63–66.
Milkov, A.V., Sassen, R., Apanasovich, T.V., Dadashev, F.G., 2003. Global gas flux from mud volcanoes: a significant source of fossil methane in the atmosphere and the ocean. Geophys. Res. Lett. 30 (2).
Mitchell, G.A., Orange, D.L., Gharib, J.J., Kennedy, P., 2018. Improved detection and mapping of deepwater hydrocarbon seeps: optimizing multibeam echosounder seafloor backscatter acquisition and processing techniques. Mar. Geophys. Res. 39 (1–2), 323–347.
Orcutt, B.N., Boetius, A., Lugo, S.K., MacDonald, I.R., Samarkin, V.A., Joye, S.B., 2004. Life at the edge of methane ice: microbial cycling of carbon and sulfur in Gulf of Mexico gas hydrates. Chem. Geol. 205, 239–251.
Roberts, H.H., 2001. Fluid and gas expulsion on the Northern Gulf of Mexico continental slope: mud-prone to mineral-prone responses. In: Paull, C.K., Dillon, W.P. (Eds.), Natural Gas Hydrates: Occurrence, Distribution, and Detection. In: Geophysical Monograph Series, vol. 124. AGU, Washington, DC, p. 315.
Roberts, H.H., Shedd, W., Hunt, J., 2010. Dive site geology: DSV ALVIN (2006) and ROV JASON II (2007) dives to the middle-lower continental slope, northern Gulf of Mexico. Deep-Sea Res., Part 2, Top. Stud. Oceanogr. 57, 1837–1858.
Römer, M., Sahling, H., Pape, T., Bahr, A., Feseker, T., Wintersteller, P., Bohrmann, G., 2012. Geological control and magnitude of methane ebullition from a high-flux seep area in the Black Sea—the Kerch seep area. Mar. Geol. 319, 57–74.
Rooze, J., Peterson, L., Peterson, R.N., Meile, C., 2020. Porewater flow patterns in surficial cold seep sediments inferred from conservative tracer profiles and early diagenetic modeling. Chem. Geol. 119468.
Ruppel, C., Dickens, G., Castellini, D., Gilhooly, W., Lizarralde, D., 2005. Heat and salt inhibition of gas hydrate formation in the northern Gulf of Mexico. Geophys. Res. Lett. 32.
Römer, M., Hsu, C.W., Loher, M., MacDonald, I., dos Santos Ferreira, C., Pape, T., Mau, S., Bohrmann, G., Sahling, H., 2019. Amount and fate of gas and oil discharged at 3400 m water depth from a natural seep site in the southern Gulf of Mexico. Front. Mar. Sci. 6, 700.
Simonetti, A., Knapp, J.H., Sleeper, K., Lutken, C.B., Macelloni, L., Knapp, C.C., 2013. Spatial distribution of gas hydrates from high-resolution seismic and core data, Woolsey Mound, Northern Gulf of Mexico. Mar. Pet. Geol. 44, 21–33.
Smith, A.J., Flemings, P.B., Fulton, P.M., 2014. Hydrocarbon flux from natural deepwater Gulf of Mexico vents. Earth Planet. Sci. Lett. 395, 241–253.
Solomon, E.A., Kastner, M., Jannasch, H., Robertson, G., Weinstein, Y., 2008. Dynamic fluid flow and chemical fluxes associated with a seafloor gas hydrate deposit on the northern Gulf of Mexico slope. Earth Planet. Sci. Lett. 270, 95–105.
Sommer, S., Pfannkuche, O., Linke, P., Luff, R., Greinert, J., Drews, M., Gubsch, S., Pieper, M., Poser, M., Viergutz, T., 2006. Efficiency of the benthic filter: biological control of the emission of dissolved methane from sediments containing shallow gas hydrates at Hydrate Ridge. Glob. Biogeochem. Cycles 20 (2).
Sultan, N., Marsset, B., Ker, S., Marsset, T., Voisset, M., Vernant, A.M., Bayon, G., Cauquil, E., Adamy, J., Colliat, J.L., Drapeau, D., 2010. Hydrate dissolution as a potential mechanism for pockmark formation in the Niger delta. J. Geophys. Res., Solid Earth 115 (B8).
Teske, A., Joye, S.B., 2020. The Gulf of Mexico: an introductory survey of a seep-dominated seafloor landscape. In: Marine Hydrocarbon Seeps. Springer, Cham, pp. 69–100.
Wang, B., Socolofsky, S.A., Breier, J.A., Seewald, J.S., 2016. Observations of bubbles in natural seep flares at MC 118 and GC 600 using in situ quantitative imaging. J. Geophys. Res., Oceans 121 (4), 2203–2230.
Wang, Z., Stout, S.A., 2007. Oil Spill Environmental Forensics: Fingerprinting and Source Identification, 1st ed. Academic Press, p. 620.
Wankel, S.D., Joye, S.B., Samarkin, V.A., Shah, S.R., Friederich, G., Melas-Kyriazi, J., Girguis, P.R., 2010. New constraints on methane fluxes and rates of anaerobic methane oxidation in a Gulf of Mexico brine pool via in situ mass spectrometry. Deep-Sea Res., Part 2, Top. Stud. Oceanogr. 57, 2022–2029.
Weber, T.C., Mayer, L., Beaudoin, J., Jerram, K., Malik, M., Shedd, B., Rice, G., 2012. Mapping gas seeps with the deepwater multibeam echosounder on Okeanos Explorer. Oceanography 25 (1-Supplement).
Wilson, R.M., Macelloni, L., Simonetti, A., Lapham, L., Lutken, C., Sleeper, K., D'Emidio, M., Pizzi, M., Knapp, J., Chanton, J., 2014. Subsurface methane sources and migration pathways within a gas hydrate mound system, Gulf of Mexico. Geochem. Geophys. Geosyst. 15, 89–107.
Woolsey, M., Woolsey, A., Hulme, S., 2015. AUV-derived geographical photomosaics-using multibeam bathymetry to correct image placement. In: OCEANS'15 MTS/IEEE Washington. IEEE, pp. 1–7.